

promoting access to White Rose research papers



Universities of Leeds, Sheffield and York
<http://eprints.whiterose.ac.uk/>

This is an author produced version of a paper published in **Journal of Molecular Biology**.

White Rose Research Online URL for this paper:
<http://eprints.whiterose.ac.uk/3456/>

Published paper

Burgess, S.A., Yu, S., Walker, M.L., Hawkins, R.J., Chalovich, J.M. and Knight, P.J. (2007) *Structures of smooth muscle myosin and heavy meromyosin in the folded, shutdown state*, *Journal of Molecular Biology*, Volume 372 (5), 1165 - 1178.

**STRUCTURES OF SMOOTH MUSCLE MYOSIN AND HEAVY MEROMYOSIN
IN THE FOLDED, SHUTDOWN STATE**

Stan A. Burgess^{1,2}, Shuizi Yu^{1,2}, Matt L. Walker^{1,2}, Rhoda J. Hawkins^{2,3}, Joseph M.
Chalovich⁴, Peter J. Knight^{1,2}

¹Institute of Molecular and Cellular Biology, Faculty of Biological Sciences, University of Leeds, LS2 9JT, U.K.

²Astbury Centre for Structural Molecular Biology, University of Leeds, LS2 9JT, U.K.

³IRC in Polymer Science and Technology, School of Physics and Astronomy, University of Leeds, LS2 9JT, U.K.

⁴East Carolina University School of Medicine, Greenville, NC 27858-4354, U.S.A.

Corresponding author:

Dr Peter J. Knight

Faculty of Biological Sciences

LC Miall Building

University of Leeds

Leeds LS2 9JT

UK

Telephone: +44 113 3434349

Fax: +44 113 3431935

Email: p.j.knight@leeds.ac.uk

Running title: Structure of shutdown smooth muscle myosin

Keywords: myosin, smooth muscle, regulation, electron microscopy, image processing

Abbreviations: ELC, essential light chain; HMM, heavy meromyosin; RLC, regulatory light chain.

S. Yu's present address is Biotechnological Center, University of Technology, Dresden Pfotenhauerstrasse 108, Dresden D-01307, Germany.

M.L. Walker's present address is MLW Consulting, 11 Race Hill, Launceston, Cornwall PL15 9BB, UK.

R.J. Hawkins' present address is FOM Institute for Atomic and Molecular Physics,
Kruislaan 407, 1098 SJ Amsterdam, The Netherlands.

ABSTRACT

Remodelling of the contractile apparatus within smooth muscle cells is an essential process that allows effective contractile activity over a wide range of cell lengths. The thick filaments may be redistributed via depolymerisation into inactive myosin monomers that have been detected *in vitro*, in which the long tail has a folded conformation. The structure of this folded molecule has been controversial. Using negative stain electron microscopy of individual folded molecules from turkey gizzard we show they are more compact than previously described, with heads and the three segments of the folded tail closely packed. Smooth muscle heavy meromyosin (HMM), which lacks two-thirds of the tail, closely resembles the equivalent parts of whole myosin. Image processing reveals a characteristic head region morphology for both HMM and myosin whose features are identifiable by comparison with less compact molecules. The two heads associate asymmetrically: the tip of one motor domain touches the base of the other, resembling the blocked and free heads of this HMM when it forms 2-D crystals on lipid. The tail of HMM lies between the heads, contacting the blocked motor domain, unlike in the 2-D crystal. The tail of the intact myosin is bent sharply and consistently at two positions close to residues 1175 and 1535. The first bend position correlates with a skip in the coiled coil sequence, the second does not. The first segment runs between the heads from the head-tail junction. Unexpectedly, the other segments associate only with the blocked head rather than both heads, such that the second bend lies at a specific position near the C-lobe of the blocked head regulatory light chain. Quantitative analysis of tail flexibility shows that the single coiled coil of HMM has an apparent Young's modulus of about 0.5 GPa. The folded tail of the intact molecule is less flexible indicating interactions between the segments. The folded tail does not modify the compact head arrangement but stabilises it, indicating a structural mechanism for the very low ATPase activity of the folded molecule.

INTRODUCTION

Myosin 2 is a large protein comprising two 16-nm heads attached to one end of a 155-nm tail. The classical state of this myosin is a polymer, the thick filament, in which the tails of many molecules pack closely together to form the filament backbone, with the heads arrayed on the surface¹. A remarkable property of the myosin 2 molecule is its ability, in certain conditions, to fold into a more compact form as an alternative to polymerisation. This increases the sedimentation coefficient from 6S, typical of myosin with an extended tail, to 10S. Folding was initially described for smooth muscle myosin and non-muscle myosins^{2;3;4}, and has also been detected in striated muscle myosins from rabbit⁵ and scallop⁶. Interconversion between filaments and a folded monomer pool may be critical to the ability of smooth muscle to adapt for generating force over a wide range of lengths⁷.

Electron microscopy after metal shadowing shows that the folded molecule has a characteristic shape: the ~155 nm tail is folded or looped into three roughly equal segments, with folding at the first bend bringing the second bend close to the heads, and the third segment frequently crossing the heads near the head-tail junction. It has generally been assumed that the folded tail interacts roughly equivalently with both heads. This notion received support from crosslinking data that led to a model in which the second bend happens as the tail passes over the head-tail junction, making similar interactions with both heads⁸. However there is no direct evidence for this arrangement. The tightness of folding is variable, and since the shadowing method may cause structural rearrangements⁹ the true structure of the molecule under physiological conditions has been unclear. The heads tend to be flexed back along the tail (the heads-down orientation) rather than randomly oriented. However, the images showed considerable heterogeneity in both the head orientation and the path of the tail³.

The folded conformation correlates with regulation of myosin enzymatic and motor activity. The motor domain of myosin is formed by the N-terminal half of a 220 kDa heavy chain which continues through a lever domain as a long α -helix in association with essential (ELC) and regulatory (RLC) light chains¹⁰ (Fig. 1A). Smooth muscle and non-

muscle myosin 2 are switched on by phosphorylation of their RLCs by a specific kinase. Dephosphorylation abolishes movement of actin and activation of myosin ATPase by actin, and the ATPase of the myosin alone is also reduced. Over a range of ionic strengths similar to physiological and with ATP present, dephosphorylation *in vitro* favours the folded molecule, at the expense of thick filaments⁹. Folded myosin has almost no ATPase activity, and both active sites are occupied by very tightly bound ADP and phosphate^{6;11}. For both smooth muscle myosin filaments and proteolytically-truncated smooth muscle myosin (heavy meromyosin or HMM; Fig. 1A) such trapping of products is less marked^{11;12}, but both the heads-down conformation and ATPase in the absence of actin show a dependence on ionic strength that allows a low ATPase to be correlated with the heads-down conformation. Thus the folded molecule is a shutdown state in which both ATPase activity and polymerisation properties are suppressed.

The structural basis of tail folding is not understood. The tail is formed by the C-terminal halves of the two identical heavy chains winding together as an α -helical coiled coil (Fig. 1A). Although the tail is gently flexible throughout its length there are discrete positions where much sharper bending is seen^{5;13}. The origins and roles of such bends are unclear, but they may originate from local weakening of the coiled coil by additional, ‘skip’ residues (Fig. 1A) which perturb the heptad pattern of amino acid residues that stabilises the coiled coil conformation¹⁴.

A detailed structural description of the shutdown state is needed to understand control of myosin 2 activity. 3-D density maps of the arrangement of the heads in 2-D crystals of smooth muscle HMM and full-length myosin on lipid monolayers have been produced by electron cryo-microscopy at a resolution of 2 nm, and atomic models of myosin heads and parts of the tail were fitted into them^{15;16;17}; Fig. 1B). An unexpected asymmetry was found in the interaction between the heads in the shutdown state: the tip of one, so-called ‘blocked’ head is in contact with the motor domain-ELC junction region of the other, ‘free’ head. A very similar arrangement of heads occurs in switched off *Tarantula* thick filaments¹⁸. Unfortunately, most of the tail is not visible in the 2-D crystal density maps. The position of the coiled-coil domain to the side of the heads rather than between

them was unexpected, and has been questioned ¹⁹. There was no evidence that the tail of the full length myosin was still folded in the 2-D crystal, so the folded (10S) monomer could have a quite different head arrangement. A cryo-atomic force microscopy study of single molecules failed to detect the same structure and concluded that any interaction between the heads was very weak ²⁰. Moreover, switched-on HMM, thought to have a wide range of head movement in solution, also produced crystalline packing, but with an intermolecular rather than intramolecular contact between heads ¹⁶, suggesting that the structure of the shutdown state adopted in the 2-D crystal might also be only one of many structures present in solution.

For single folded myosin molecules basic questions therefore remain: what are the shapes and arrangement of the two heads, and what is the structure and path of the folded tail? In the present work we address these questions using negative staining and single particle image processing to study individual molecules of shutdown smooth muscle myosin and HMM. We have imaged other myosins by this method as it allows better control of the solution conditions around the molecules and reveals greater detail than shadowing ^{5; 21; 22; 23; 24}.

RESULTS

Negatively-stained, switched-off smooth muscle myosin shows a structure that has rarely been seen by the shadowing method. Instead of two separate heads attached to a tail that is looped back to the heads, a more compact molecule is common (Fig. 2A, B). The heads are closely apposed and the tail, reduced to about a third of its fully-extended length by folding at two points, forms a single structure. This compact structure is abundant in fresh preparations, and most other molecules show two separate heads on a compactly-folded tail. As a preparation ages, these less compact molecules become increasingly common, some molecules have unfolded tails, and short filaments (polymers) are seen (unpublished data). This suggests that the compact structure is the native structure under these low ionic strength conditions, but is labile in storage.

HMM forms a similar compact structure of closely-apposed heads attached to a short tail (Fig. 2C, D). The structure is more common at lower ionic strength, and with a short incubation time on the carbon film of the electron microscope grid before staining, indicating that it is less stable than for full-length myosin.

Galleries of raw images of both whole myosin (Fig. 2B) and HMM (Fig. 2D) suggest consistency in structure of compact molecules, but variation in structure and staining makes objective description difficult. Therefore we have used single particle image processing methods to analyse these structures. The structure of the HMM head region is described first due to its relative simplicity, followed by that of the compact structure of whole myosin.

Heads of HMM

Image processing reveals a detailed structure for the head region of compact HMM (Fig. 3). The images are primarily one view of the molecule, which evidently has a strongly preferred orientation of adsorption onto the carbon film. Classification based only on features within the heads and the nearby tail produces many well-populated classes that differ largely in staining rather than molecular structure (Fig. 3A-C). In all classes the tail emerges near the middle of the base of the roughly triangular head region, and fades

progressively in the averages due to its variable shape (see below). The head region is subdivided into domains surrounding a central pool of stain. To the right of the tail is a pale triangular domain, boldly outlined by stain, consistent in size and shape with a motor domain seen end on. Above it are smaller domains that could be the associated ELC and RLC domains. To the left of the tail the structure is different. The shape and size suggest a motor domain in side view with its associated ELC and RLC forming the upper left side of the triangular head region. Other class averages of HMM molecules show more variability in structure. The motor domain of the right head often adopts a slightly different orientation (Fig. 3D & E) from the strictly compact form. Less often, both heads appear less compact (Fig. 3F)

HMM molecules with heads less closely apposed establish the assignment of domains (Fig. 4). A scatter plot of head angles shows that while either head adopts a wide range of angles to the tail, in most molecules the angles are small. Image averages of subclasses of molecules clustered near the origin of the plot reveal some in which the left head is in the compact position, while the right head has swung away from the tail, and *vice versa* (Fig. 4, lower panels). It is clear that the tail runs straight up through the central stain pool to the top of the molecule, which locates the RLC of each head to that position, and shows that both heads are in a 'heads down' orientation relative to the tail. These images also establish that our identification of the motor domains of the compact molecule is correct. Therefore the upper left side of the triangular head region is the light chain domain of the left head, the lower left side is the motor domain of the left head and the right side is the right head. Where the left head has swung away, the tail lies beside the right motor domain, whereas when the right head has swung away, the tail crosses the tip of the left motor domain. This suggests there are sites of interaction between the tail and both motor domains. There is no gap between the RLCs of the two heads in either compact or partially-opened molecules, but on the contrary, stain is effectively excluded. This suggests the two RLCs overlap, as has previously been suggested in a model structure of the head-tail junction in which the tail is a fully-formed coiled coil²⁵.

The compact structure of the heads is very similar to that obtained from 2-D crystals^{16;17} (Fig. 1B). Importantly, our interpretation of the single molecule images is unambiguous and independent of the data of Wendt *et al.* The ‘blocked’ head of Wendt *et al.* corresponds to the left head in our images, and the ‘free’ head to the right one. Our data show that the asymmetry seen by them is not an artefact of crystallisation, but is the true structure of the shutdown heads.

The path of the tail in HMM differs markedly from that reported by Wendt *et al.*¹⁷. It lies between the two heads, as expected for a heads-down structure of the molecule, rather than angled across the RLC of the free head, then bent sharply to run towards the free head motor domain (Fig. 1B). Thus, while the structure of the heads agrees well with the crystallized molecules, the structure of the tail is fundamentally different, but is consistent with the earlier shadowing studies.

Heads of full-length myosin

Classifying the head region of images of whole myosin molecules produced detailed averages (Fig. 5), which can be readily interpreted by comparison to HMM molecules (Figs 3 and 4). The triangular shape formed by the two heads in the compact structure of HMM is clearly recognisable in the whole molecule, and is seen in a similar view (Fig. 5A-C). However, the detail in the free head is greater, indicating that the compact structure of whole myosin is less variable. Additional mass is seen in the head region, due to the presence of the folded tail (see below). Nevertheless, it is clear that the heads of folded myosin adopt a conformation very similar to HMM, so they are not much perturbed by interactions with the folded tail. In addition to this typical orientation of the molecule on the carbon film (~80% of all compact, well-stained molecules), myosin was also found on its side (~20%), an example of which is shown in Fig. 4D and also, very rarely, upside-down (<3%, unpublished data).

Some classes of the head region show the heads in a less compact structure (Fig. 5E & F). These show that the motor domain of the free head can swing out and in some cases the whole head swings out at the head-tail junction. The appearance of the motor domain is

different in such molecules, suggesting the conformation within the head has changed (see especially Supplementary Movie 1). The blocked head is little changed from its appearance in compact molecules, indicating that in the whole molecule its conformation is the more stable of the two heads, presumably due to more extensive interactions with the tail.

Path of the tail within the head region

The similarity of the shapes and arrangement of heads in whole myosin and HMM allows additional features of the head region of myosin images to be ascribed to the folded tail. Close to the emergence point of the tail of HMM from the head region, a single, bold structure is produced by the coalescence of the three segments of the folded tail (arrow, Fig. 5B). The paths of the tail segments within the head region are less clear owing to superposition of structures. However, one segment can be followed around the perimeter of the blocked head motor domain and ELC until it terminates in a prominent spot adjacent to the C-lobe of the RLC (arrowhead, Fig. 5B).

The path of the tail within the head region is shown by subtracting an image average of HMM from one of myosin (Fig. 6). The subtraction image reveals a line of material of variable prominence that runs across the blocked head, connecting the prominent spot (Fig. 6, arrowhead) to the coalesced tail (Fig. 6, arrow). It also shows more clearly the section of tail running around the periphery of the blocked head. It is clear that the prominent spot marks the position of a sharp bend in the tail, and it is plausible that the section of tail revealed in the subtraction image runs over the top of the myosin head, allowing it to be obscured in some places by stain accumulating between it and the carbon film. It is clear that contrary to expectation, the folded tail lies to one side of the head-tail junction, and does not interact with the free head.

Because the three segments of tail coalesce, we cannot be sure from our images alone whether it is segment 2 or 3 that runs around the periphery of the blocked head, though in some classes (Fig. 7E) this segment appears to extend towards the first bend suggesting it is segment 2. This assignment is supported by the appearances of molecules shadowed

after drying on mica, where the tail often forms an open loop. Here it is segment 2 that lies beside the head and segment 3, distal to the second bend, that lies across the head region, in contact with the light chain domain ^{2,3;26}.

Tail of HMM outside the head region

Classification of the tail portion of HMM reveals a diversity of tail shapes (Fig. 7A). The structures of the head region are invariant among these classes, showing that tail shape is not correlated with head structure. In each class the tail emerges from close to the meeting point of the two motor domains, becoming smoothly curved more distally. The tail fades towards the tip, indicative of the diversity of paths taken, and precluding measurement of tail length. The central panels of the group show almost straight tails; tails curving left or right are less common (Fig. 7B) and appear more heterogeneous. The angle distribution is centred at 10.6° rather than 0° (Fig. 7B), probably reflecting a small error in locating the head-tail junction for the reference axis, rather than a kink in the tail.

The distribution of tail angles suggests that the images record a spring-like flexion of the coiled coil, tethered on the motor domains rather than at the head-tail junction (see also Supplementary Movie 2). The thermally-driven, spring-like properties of the tail are quantified by the standard deviation (15.3°) of the angle distribution. The apparent Young's modulus of the coiled coil derived from that value is 0.53 GPa (GJ.m^{-3} ; see Methods).

Structure of full-length tail outside the head region

Classification of the tail region of images of whole myosin (Fig. 7C) shows that the folded tail is less flexible than the single tail of HMM (see also Supplementary Movie 3). In whole myosin, the tail region broadens and is usually less strongly outlined by stain beyond the coalesced region, presumably because the three tail segments lie side-by-side on the carbon film. The coalesced region is angled to the right, and the classes show a range of further rightward bending of the tail distal to this, with a mean angle of 22.0° (Fig. 7D). Compared to the tail of HMM, the folded myosin tail shows a smaller range of angles (standard deviation 7.5°), and tails are not seen bending to the left. Both features

indicate that constraints are imposed by interactions between tail segments.

Interpretation of the observed range of angles in terms of the Young's modulus of the folded tail is clouded by the diversity of structures present in the averages, some of which may be the result of unwinding of a more compact structure through absorption on the carbon film of the EM grid (see Discussion).

Structure within the folded tail is seen better by classifying images aligned using the tails as well as the heads (see Materials and Methods; Fig. 7E). The distal end of the folded tail has a characteristic structure. The shorter, right side typically ends abruptly with a brighter spot (arrowhead, Fig. 7E). By analogy with the prominent spot seen in the head region (Fig. 5), this strongly suggests the tail is bent back on itself here to form the junction between segments 1 and 2 (Fig. 8 position 1175). On the left side the tail extends further (typically 6.6 nm, arrow Fig. 7E) and usually more weakly, as expected for the single coiled coil of segment 3. That this segment always lies to the left of the first two is an indication that the three segments of the tail make a specific structure (this is also clear in Supplementary Movie 4). The tail segments are too closely apposed to resolve consistently as separate strands, and a class is seen (asterisk, Fig. 7E) in which they are coalesced throughout their length rather than spread. In this class the structure is straighter than the spread tails in other classes, and its long axis extrapolates through the prominent spot (the second bend) on the other side of the blocked head. These features suggest that there are interactions between the tail segments that make the structure rigid.

The clarity of the image averages of the tails allows precise measurements of tail segment length (Fig. 8). These agree with previous observation of shadowed molecules in showing that segment 3 is longer than segment 2^{2; 3; 26}.

DISCUSSION

We have analyzed the structure of the shutdown state of smooth muscle myosin by negative stain electron microscopy of single molecules. Our analysis shows the disposition of the heads in the folded molecule for the first time. The arrangement closely resembles that reported earlier for molecules in 2-D crystals and is therefore unaltered by interactions with the folded tail and loss of crystal contacts. Compared to the crystals we find differences in the tail region of myosin, and show for the first time the course of the folded tail. These differences probably result from certain advantages that the analysis of single molecules has over crystals. In particular it permits unambiguous assignment of densities to an individual molecule, it avoids intermolecular contacts and interaction with lipid, both of which may perturb the structure and it allows large scale flexibility of the molecule to be observed which is necessarily suppressed by crystallisation.

Structure of shutdown heads

Detailed structures have been proposed for the head regions of HMM and whole myosin molecules based on fitting atomic structures to densities in 2-D crystals^{15;17}. We find a very similar structure in single HMM molecules and more importantly in whole myosin in which the tail is folded and interacting with the head region, which has probably not been examined hitherto (*contra* Liu et al.¹⁵, see below). This structure is therefore physiologically relevant. Blocked-head densities were well fitted by an atomic structure of a smooth muscle myosin motor domain and ELC²⁷, which has ADP.AIF₄ bound in its active site (i.e. the ‘closed’ conformation), and which additionally is strongly bent at the junction of the motor domain and lever by disruption of the heavy chain α -helix at the ‘pliant region’²⁸. Free-head densities could only be fit if the bending of this structure at the pliant region was reduced, creating a structure intermediate between this and the scallop striated muscle myosin closed structure in which the pliant region is an undistorted α -helix²⁸. These observations suggest that the free head when in contact with the blocked head adopts a conformation not yet known in atomic detail. It is unlikely to be a post-rigor-like ‘open’ head conformation because we have found that post rigor atomic structures are not good fits to our images of compact molecules (unpublished data).

It is notable that the free head appears to be the more mobile of the two heads in whole myosin (Fig. 5), and that when it is detached from the blocked head its motor domain adopts a different orientation. We find that where the free head is just separate from the blocked one (Fig. 5E & F; Supplementary Movie 1), it cannot be matched by any orientation of any closed crystal structure (unpublished data). Instead it is better matched by the open head structure of either chick or scallop myosin^{10;28} in an orientation that approximately retains the RLC and ELC positions of the Wendt et al. model. We have previously shown that myosin 5 heads populate both open and closed conformations in the presence of ATP²⁴. These observations suggest that the closed conformation of the head can form the compact structure, but switching to the open conformation disrupts the contacts between the motor domains. Our data further suggest that the blocked head, due to extensive interactions with the tail, is limited to the closed conformer.

The failure of cryo-AFM to detect the compact head structure of smooth muscle myosin²⁰ probably arose from the specimen preparation procedure used. In our negative stain experiments, the compact structure was revealed only with a very brief incubation of HMM on the carbon film before uranyl acetate fixation; with longer incubation the heads were separated. Since specimen preparation for cryo-AFM was done under conditions that favoured an extended rather than folded tail, it was comparable to our experiments on HMM rather than the more stable folded myosin, and it is likely therefore that the heads became separated. We should expect the compact head structure *in vivo* to involve only weak interactions of the heads with each other and the tail, otherwise it would be too difficult to activate the molecule. This explains why it is easily disrupted *in vitro*.

Structure of the head-tail junction

At the head-tail junction we find continuous stain exclusion rather than two lobes, which suggests that the N-terminal domains of the two RLCs abut or overlap. Wendt *et al.*¹⁷ and Liu *et al.*¹⁵ also found continuous density in their 3-D maps. However in their deposited model (PDB: 1I84) there is no overlap between the RLCs, so the model does not fill the density contour shown (Fig. 1C of ref¹⁷), and there is a gap between them in

the view of the model that corresponds to the view we see (Fig. 1B). The refined model¹⁵ brings the N-terminal domains together by allowing more freedom of movement of the lever relative to the motor domains. This modelling used levers based on the chicken skeletal crystal structure¹⁰, but it is likely that the levers can flex at several points along their length^{25; 29} implying that the shapes of the off-state myosin levers differ from existing atomic structures and possibly from one another.

The N-terminal 24 residues of each RLC (including the phosphorylatable Ser19 that controls activity) are not included in any atomic structures, yet together constitute ~5.4 kDa and so could contribute to stain exclusion. They are required for formation of the folded molecule and for control of ATPase activity³⁰, and crosslinks can be made between this part of the RLC and the RLC of the other head in switched-off molecules^{8; 31}. However the tertiary structure of this sequence in the intact molecule remains unknown, so it is unclear how it contributes to the observed structure. A single head partnered by the light chain domain of another head is poorly regulated³², indicating that although interactions between the two light chain domains are involved in regulation, both motor domains are required for full regulation of actin activation.

It has been proposed that the two RLC's overlap extensively because crosslinking occurs between the N-terminal lobe of one RLC and the C-terminal lobe of the other⁸. The structure proposed to account for these results is symmetrical, and not consistent with our images, because it brings the ELC's too close together. Since Wahlstrom et al.⁸ have no evidence for symmetrical crosslinking, it is possible that their results could be consistent with an asymmetrical structure in which, for instance, the N-terminal lobe of the blocked head RLC abuts the C-terminal lobe of the free head RLC but not *vice versa*.

Position and folding of the tail

An unexpected finding is the marked asymmetry in the disposition of the folded tail with respect to the heads. While segments 2 and 3 of the tail take a specific path around the blocked head, no part of these segments interacts with the head-tail junction or the light chains of the free head. This shows to be wrong the assumption that grew from early

observations showing the folded tail close to the head-tail junction², that there are roughly equivalent interactions between both heads and the tail.

The model proposed for 2-D crystals of HMM¹⁷ describes a different path of the tail than we have found in isolated molecules of either HMM or whole myosin molecules. However only about 30% of the expected coiled coil was seen in this previous study. In 2-D crystals of whole myosin more coiled coil was detected, as expected, but it was in discontinuous sections amounting to about 40% of the expected length, and the molecular path could not be followed¹⁵. In that study there is no density in the 3-D map which corresponds to tail segments 2 and 3 running around and across the blocked head nor is there the strong feature where all three segments of coiled coil run together distal to the junction of the two motor domains. These differences indicate that in the 2-D crystal of whole myosin the tail was not folded in the way we have described, and may not have been folded at all, *i.e.* the molecule may not have been in the 10S conformation. What we find in single folded molecules is a straight first segment of tail that crosses the space between the two heads to emerge beyond where the two motor domains touch, and no part of the folded tail is close to the periphery of the light chains of the free head as was shown by Wendt et al.¹⁷. The relation of heads and segment 1 of the tail in our images is instead obviously related to the ‘heads-down’ structure long known from shadowing studies of this and other myosins^{3; 9; 33}.

Myosin molecules that have had one head removed by proteolysis can still adopt a hydrodynamically-compact structure when switched off³⁴. However, this folding occurs only at very low ionic strength. Our observation that the folded tail interacts primarily with the blocked head may explain how such a single-headed molecule is still able to fold. The reduced stability of folding indicates that the second head contributes to folding, possibly by stabilising the blocked head in the correct orientation to interact with the folded tail.

Tail length and paths of the tail segments

The total measured length of the tail is only 1.5 nm less than the expected length (Fig. 8), which is closer than previous studies, both from our group and others. Our data therefore suggest that the sequence is almost completely coiled coil when the heads are in the compact conformation. Consequently, the amount of heptad sequence that can give rise to density at the head-tail junction is small, and this favours the interpretation of this density as overlapping RLCs. A diagram summarizing our interpretation of the structure of the entire folded molecule is shown in Fig. 8. Because we have here described the path of the folded tail in detail for the first time, we now consider the implications of our data for the properties of each of its three segments.

The path of segment 1 of the tail in the head region of folded myosin is the same as in HMM (Fig. 6). Images of HMM molecules (Figs. 3 and 4) suggest specific interactions between the tail and both motor domains. Its path is strikingly similar to the tail in switched-off *Tarantula* thick filaments, including the location where the tail exits the head region¹⁸. The comparison allows us to infer that segment 1 lies on top of the blocked head in the view we describe. The close similarity with *Tarantula* suggests that in the thick filaments of relaxed smooth muscle a similar structure will be present, i.e. that unfolding of segments 2 and 3 and polymerisation will still allow the heads-down structure to form and be stabilised by interaction with the proximal tail.

Because the motor domains are not symmetrically arranged, their interactions with segment 1 of the tail will be different. The interactions would be 10 to 12 nm along the tail from the head-tail junction, i.e. ~80 residues of coiled coil (~12 heptads). An in-phase addition of a 32-residue (4.8 nm) leucine zipper sequence reduces regulation if the insertion point is closer than 15 heptads to the start of the heptad sequence³⁵. However, if the leucine zipper replaces native sequence within the first 15 heptads rather than being added into it, regulation is not disturbed. These results can now be better understood because addition would move the interacting tail segment 4.8 nm further from the head-tail junction, thereby disrupting interactions with the motor domains whereas substitution would not have this effect.

The distal end of segment 1 is defined by a sharp, precisely-determined bend (Fig. 7E). At 48.5 nm, this segment is longer than previous measurements of the distance from the head-tail junction to the first bend in smooth and striated muscle myosin molecules¹⁴. This indicates that it is this first segment that is partially unfolded^{14; 36} or foreshortened²⁵ in the extended molecules previously measured.

The evidence indicates that segment 2 does not simply run in a straight line from the first bend to the second, but is the segment that can be seen skirting around the blocked head. The significance of this path is unknown, but it would allow the tail to make interactions with the blocked head N-terminal SH3 sub-domain and/or the converter regions of the motor domain, and with the ELC (see Fig. 1B). In this position segment 2 might constrain the head to remain in the strongly bent conformation.

Segment 3 runs across the blocked head, lies to the left of the other two segments outside the head region and terminates up to ~7 nm beyond the first bend (Fig. 8). Onishi *et al.*²⁶ also noted a preponderance of third segments lying on the left side in molecules deposited on mica. The extension of segment 3 beyond the junction of segments 1 and 2 is a strong qualitative indication that this segment is longer than the other two, a feature that can also be seen in the metal-shadowed images of earlier studies^{3; 9; 26}.

The path of segment 3 in the head agrees well with the results of a crosslinking study which found that a link could be made in folded smooth muscle myosin between Cys108 of the RLC and residues in the tail between Leu1554 and Glu1583³⁴. Thus in the Wendt *et al.*¹⁷ model of the heads, Cys108 is on the part of the RLC surface where we find segment 3 (red arrow in Fig. 8, compare with Fig. 6). Also the distance between the second bend (close to residue 1535) and the site of heavy chain crosslinking, which would be 3 to 7 nm of coiled coil, encompasses the measured distance in image averages from the second bend to the C-lobe of the RLC (5.0 ± 0.1 nm). The location of Cys108 indicates that segment 3 lies on top of the blocked head rather than under it, as we inferred from the staining behaviour. It is probable that there is a specific interaction between segment 3 and the RLC because in shadowed molecules, where the tail is looped

across the head instead of compactly folded, it often crosses the head in a similar location and with the same polarity^{2;3}. Segment 3 crosses the RLC of the blocked head, but does not approach the RLC of the free head, explaining why only one of the two RLC's becomes crosslinked to heavy chains³⁴. Our observation that the free head is the more mobile suggests that it is this head which increases its ATPase when salt is added³⁴, whereas the crosslinked, blocked head may be constrained to remain in the closed structure, and therefore remain essentially inactive. It is a natural consequence of the structure we describe that the free head would be unaffected by the crosslinking, whereas the blocked head would be strongly constrained in the closed structure by the encircling tail, and therefore unable to execute the cycle of structural change required for ATPase activity.

By contrast, the relationship between the heads and the path of the tail we have found are not easily reconciled with recent crosslinking work suggesting a substantial antiparallel overlap of the two RLCs, and that the second bend in the tail lies over the head-tail junction^{8;37}. Possibly these crosslinks preferentially occur in a folded conformer that is not abundant in our conditions.

Interactions between tail segments

Within the head region, the three segments of tail follow largely separate paths, but segments 1 and 3 may be in contact where they cross the same face of the blocked head motor domain. A consistent feature of the folded tail is the close packing of the three segments of tail just outside the head region, and in some molecules this closeness is maintained throughout the tail region. It is not clear what causes this close association, but the images suggest the tails may twist together as a three-stranded rope. A comparison with images of partially unwound helical tubes (e.g. the tubular polymer of myosin subfragment-2³⁸), suggests that the folded tail is a helical structure that unwinds after contact with the carbon film. Unwinding appears to be to the right, consistent with the three segments forming a right-handed helix.

Interactions between the tail segments is also indicated by the reduction in flexibility of the tail between HMM and whole, folded myosin. The curvature of the tails could be dismissed as an artefact of adsorption, staining and drying, but the estimate of 0.53 GPa for Young's modulus of the HMM tail that we obtain by taking the data at face value is remarkably close to the value of 1 GPa determined for isolated myosin rods in solution by viscoelastic measurements³⁹. In fact one could argue that the true modulus could be twice what we observe in the 2D images, and therefore a very close match indeed, due to contributions from the bending out of the plane being absorbed into our in-plane distributions. Thus the tail curvature seen by electron microscopy is to be expected because the coiled coil is flexible, and our observation that the folded tail is less curved than a single tail indicates that interactions occur between the segments.

Interactions between the folded tail segments may contribute to favouring folded monomer over polymer. At low salt concentrations, folded monomers interact without unfolding to form antiparallel dimers, apparently by interactions between segment 3 of each molecule⁹, but further polymerisation is blocked. Interactions of tail segments 2 and 3 with the compact head arrangement of the folded monomer are expected to produce a steric hindrance to filament assembly and would thereby contribute to this blockade. Intramolecular interactions between the segments may be a significant additional factor because they will compete with intermolecular interactions to inhibit the more extensive interactions between molecules required for filament formation. Because there are no detailed data on the interactions between molecules in the side polar smooth muscle thick filament⁴⁰, we cannot tell whether the competition arises because the intramolecular interactions echo those between molecules in the filament or instead are of a different kind that is mutually exclusive with intermolecular association.

Origin of bends in the tail

Our data test the proposal¹⁴ that sharp bends in the tail correlate with the position of perturbations (skip residues) in the regular heptad repeat of the tail sequence. The position of the first skip residue predicts a length for segment 1 close to that observed (Fig. 8). However, the second skip residue position predicts that segment 2 would be

longer than segment 3, whereas we and others find the reverse is true. Based on our measured length of segment 2, the sequence position of the second bend would be at residue ~1535, some 56 residues upstream of the skip position (residue 1591). This mismatch would not be resolved if the identification of segments 2 and 3 in the head region was reversed, rather it would be exacerbated since the peripheral path is the longer one, so the effect would be to shorten segment 2 and lengthen segment 3, moving the second bend still further upstream of the second skip residue. We have not detected a bend in the region of the third skip residue near the tip of the tail. We conclude that skip residues are not consistently correlated with sites of sharp bending in smooth muscle myosin.

There is no obvious feature of the amino acid sequence of the tail which explains why the second bend is found close to residue 1535. Coiled-coil prediction programs detect a region of low coiled-coil probability away from skip residues, centred at residue 1465³⁴. However, this must lie in segment 2 of the tail, and will be at a distance from the first bend that places it close to where this segment coalesces with the other two segments adjacent to the motor domains, rather than at the second bend.

Can folded myosin bind to actin?

Computer modelling showed that binding of the blocked head's motor domain onto F-actin was sterically hindered by the free head's motor domain¹⁷. We find that the free head's motor domain is also hindered, in this case by the folded tail. Thus the folded molecule should bind only weakly to F-actin. This explains previous observations that in molecules trapped in the folded state by crosslinking neither head binds to actin, even under rigor conditions, and phosphorylation no longer triggers actin activation of ATPase³⁴.

Dynamic aspects of myosin folding

Although the two heads of the compact HMM or whole myosin are structurally very distinct, they are not inherently different. Therefore if the folded monomer unfolds and refolds, a blocked head can in principle switch to become the free head. It is not known

whether this switching is frequent or rare. If the kinetic properties of the blocked and free heads differ, for instance in rates of loss of ADP and Pi, the measured rates will include a contribution from the rate of switching. In the thick filament the situation is different because the tail is anchored into the backbone, and to avoid steric clashes between the heads and backbone the expectation is that switching is rare, so biphasic kinetics should be expected.

Our observation that the compact conformation of HMM is less stable than whole myosin is consistent with the poorer ability of HMM to trap ADP and Pi¹¹, which may be a consequence of frequent conformational interconversion. The close similarity of our HMM images to the head regions of the switched off *Tarantula* thick filament structure¹⁸ suggests that smooth muscle thick filaments also form a heads-down structure stabilised by interactions with the proximal tail. For smooth muscle thick filaments formed *in vitro* there is no evidence for greater stabilisation than we find for HMM, since such filaments also do not trap ADP and Pi¹¹. *In vivo*, it is possible that filament structure is different and additional factors may be present, either of which could stabilise the switched-off state, but evidence is lacking.

In the compact conformation of the molecule we find that very little of the heptad sequence is unwound. However other data suggest dynamic unwinding of the proximal coiled coil near the head-tail junction in unfolded molecules^{19; 41; 42; 43}. The fact that mere light chain phosphorylation can change the amount of coiled coil at the start of the tail suggests that little energy is required, *i.e.* that the tail conformation is poised between helical and uncoiled. However, phosphorylation induces many changes in molecular conformation⁴⁴, and by unlocking the heads will expose the head-tail junction to the chaotropic effects of the Brownian forces acting independently on the two heads.

METHODS

Protein preparation

Smooth muscle myosin Fresh turkey gizzards from a local poultry processor were rinsed in Ringer's solution and dissected free of connective tissue. Gizzards were cut into 2 cm cubes, frozen in liquid N₂ and stored at -80°C for up to 2 months. Myosin was prepared from gizzard by a modification of previous methods^{45;46}. 0.1% Triton X-100 was included in the first wash and myosin was extracted with 40 mM imidazole-HCl (pH 7.2), 8 mM ATP, 60 mM KCl, 1 mM EDTA, 100 mg/l streptomycin sulphate and 0.5 mM dithiothreitol. The final step in purification of the myosin was gel filtration on a 2.5 x 100 cm Sepharose 4B column equilibrated with 0.5 M KCl, 0.1 mM MgCl₂, 2 mM EGTA, 0.1 mM dithiothreitol, 10 mM imidazole-HCl pH 7.0. To facilitate actin removal, 50 ml of this buffer containing 5 mM ATP was run into the column prior to loading the myosin. Approximately 30 ml of 3.4 mg/ml myosin was passed through the column⁴⁷; pure myosin was in the first half of the major peak.

Heavy meromyosin (HMM) was prepared by digesting phosphorylated myosin with chymotrypsin⁴⁸. Phosphorylation protects RLCs and gives a fully-regulated HMM. To 20 mg/ml crude myosin (not subjected to gel filtration) in 25 mM NaCl, 10 mM MgCl₂, 10 mM MOPS pH 7.0, 0.1 mM EGTA, 3 mM NaN₃ and 1 mM dithiothreitol was added an additional 15 mM MgCl₂, 0.4 mM CaCl₂, 10 nM calmodulin, 5 mM ATP and myosin light chain kinase (when needed). After 5-10 minutes (determined by a time course of a test sample) sufficient 5 M NaCl and 0.5 M EGTA were added to give 0.55 M NaCl and 6 mM EGTA. Chymotrypsin was added to give 0.1 mg/ml. After 5-10 minutes (determined by a test digestion) the cleavage was stopped by addition of PMSF to 0.02 mg/ml from a 34 mg/ml stock in isopropanol. Dephosphorylation of the HMM occurred during the dialysis steps following digestion. The final HMM was purified on either a Sephacryl S-400 or S-300 column and concentrated with an Amicon concentrator. Preparations of both myosin and HMM were tested for phosphorylation by running glycerol urea gels. Gels were normally 10% polyacrylamide containing 37% glycerol and the protein samples contained 6 M urea. In some cases 7.5% polyacrylamide glycerol urea gels were purchased from Jule Inc. (Milford, CT, USA). The levels of RLC phosphorylation of myosin and HMM were <5% prior to shipping. Proteins were

shipped between labs in wet ice to ensure a constant temperature of 0°C, then flash frozen by dropping 25 µl drops into a bath of liquid N₂. The frozen beads were stored at -196°C.

Electron microscopy

Negative stained grids were prepared using thin carbon films treated with UV light to improve preservation of myosin heads in stain⁴⁹. Thawed myosin was diluted first into an ATP-containing high salt solution, then further diluted to ~10 nM with a low ionic strength solution to induce the monomeric myosin-nucleotide complexes to fold to the 10S conformation. Final solution composition was 100 mM KCl, 2 mM MgCl₂, 1 mM EGTA, 0.15 mM ATP, 10 mM Imidazole-HCl, pH 7.0. 5 µl protein sample was applied to the carbon film and stained after a few seconds with 1% uranyl acetate without any intermediate rinse. HMM was diluted to ~10 nM in the same solution except the KCl was 20 mM, and stain was applied to the grid as quickly as possible after the protein.

Micrographs were recorded at ~40,000x using a Jeol 1200EX microscope. Calibration of magnification used the 14.4 nm spacing of paramyosin filaments⁵⁰.

Image processing

Micrographs were digitised on a Leafscan-45 densitometer (Leaf Systems, Inc., Southborough, MA) at a pixel size corresponding to 0.514 nm in the specimen. Molecules were selected interactively (by choosing the centre of the head complex), windowed out and imported into the SPIDER suite of software for image processing.

89 micrographs generated 4,400 apparently compact myosin molecules and 95 micrographs generated 1,371 apparently compact HMM molecules. For alignment, these two data sets comprising images 200x200 pixels (i.e. 103 nm square) were combined and a central region of 80x80 pixels, containing the heads, was aligned using reference-free methods⁵¹. The resulting rotations and shifts were applied to the larger images, which show well-aligned heads but variable tail positions, and are thus referred to as head-aligned images. Myosin and HMM images were then classified (together) into 96 classes and those showing successful alignment were processed further. This generated 2067

and 869 images respectively of face views (see Figs. 3 and 5A-C). All classifications were done using K-means clustering⁵². Successfully aligned HMM images were then further classified into 30 classes, producing a mixture of structures including compact and partially opened forms (see Figs. 3D-F and 4). The compact forms (5 classes, n=226) were combined and reclassified into 3 classes (Fig. 3A-C). Successfully aligned myosin images were also further classified into 56 classes, again producing a mixture of structures plus some residual misaligned images. From these, 24 classes (corresponding to 933 individual images) were selected showing good staining and both compact and open forms. These were again classified into 8 classes, 5 of which are shown (Fig. 5A-C, E & F). Side views of myosin were also found after the first classification (n=199 images). One class is shown (Fig. 5D).

To better resolve features in the tails, a separate reference-based alignment was performed using the full-sized images of myosin molecules, and using as a reference a class average showing the tail clearly (see Fig. 7E).

A total of 411 HMM molecules showing open heads and clear tails were also selected and windowed. These were manually aligned to centre the head-tail-junction and to orient the tails downwards. The angles of the two heads relative to the tail were then determined manually for each individual molecule using the computer mouse to locate the tip of each motor (see Fig. 4).

Calculation of Young's Modulus of the tail

For a microscopic, cylindrical rod, bending with thermal energy, a combination of the Equipartition Theorem and the mechanics of the bending beam produces the relation:

$$Y = \frac{l_0 k_B T}{\pi r^4 \sigma_{\theta c}^2}$$

where Y is Young's modulus of the material, l_0 is the length of the rod, k_B is Boltzmann's constant, T is absolute temperature and r is the radius of the rod. $\sigma_{\theta c}$ is the standard deviation of the distribution of angles of bending (θc) expressed in radian measure, and

corrected to a constant contour length of rod (25.7 nm) from angle measurements (θ) made at a constant chord length of 50 pixels (25.7 nm; see Fig. 7). This correction assumes the tail bends into a circular arc, from which it follows that $\theta c = \sin\theta$. We used a value of 1 nm for the radius of the coiled-coil HMM tail.

ACKNOWLEDGEMENTS

We thank Drs Christine Cremo, Kevin Facemyer, Gerald Offer and Mary Pato for stimulating discussions and Mr Michael Vy-Freedman for assistance in preparing proteins. This work was supported by a Biotechnology and Biological Sciences Research Council (UK) grant to PJK and Prof J. Trinick, and by grant AR35216 from the National Institutes of Health to JMC.

REFERENCES

1. Craig, R. & Woodhead, J. L. (2006). Structure and function of myosin filaments. *Curr. Opin. Struct. Biol.* **16**, 204-212.
2. Craig, R., Smith, R. & Kendrick-Jones, J. (1983). Light-chain phosphorylation controls the conformation of vertebrate non-muscle and smooth-muscle myosin molecules. *Nature* **302**, 436-439.
3. Onishi, H. & Wakabayashi, T. (1982). Electron-microscopic studies of myosin molecules from chicken gizzard muscle. 1. The formation of the intramolecular loop in the myosin tail. *J. Biochem. (Tokyo)* **92**, 871-879.
4. Trybus, K. M., Huiatt, T. W. & Lowey, S. (1982). A bent monomeric conformation of myosin from smooth-muscle. *Proc. Natl. Acad. Sci. USA* **79**, 6151-6155.
5. Walker, M., Knight, P. & Trinick, J. (1985). Negative staining of myosin molecules. *J. Mol. Biol.* **184**, 535-542.
6. Ankrett, R. J., Rowe, A. J., Cross, R. A., Kendrick-Jones, J. & Bagshaw, C. R. (1991). A folded (10 S) conformer of myosin from a striated-muscle and its implications for regulation of ATPase activity. *J. Mol. Biol.* **217**, 323-335.
7. Seow, C. Y. (2005). Myosin filament assembly in an ever-changing myofilament lattice of smooth muscle. *Am. J. Physiol. Cell. Physiol.* **289**, C1363-C1368.
8. Wahlstrom, J. L., Randall, M. A., Lawson, J. D., Lyons, D. E., Siems, W. F., Crouch, G. J., Barr, R., Facemyer, K. C. & Cremo, C. R. (2003). Structural model of the regulatory domain of smooth muscle heavy meromyosin. *J. Biol. Chem.* **278**, 5123-5131.
9. Trybus, K. M. & Lowey, S. (1984). Conformational states of smooth-muscle myosin - effects of light chain phosphorylation and ionic-strength. *J. Biol. Chem.* **259**, 8564-8571.
10. Rayment, I., Rypniewski, W. R., Schmidtbase, K., Smith, R., Tomchick, D. R., Benning, M. M., Winkelmann, D. A., Wesenberg, G. & Holden, H. M. (1993). 3-Dimensional structure of myosin subfragment-1 - a molecular motor. *Science* **261**, 50-58.
11. Cross, R. A., Jackson, A. P., Citi, S., Kendrick-Jones, J. & Bagshaw, C. R. (1988). Active-site trapping of nucleotide by smooth and non-muscle myosins. *J. Mol. Biol.* **203**, 173-181.
12. Suzuki, H., Stafford, W. F., Slayter, H. S. & Seidel, J. C. (1985). A conformational transition in gizzard heavy-meromyosin involving the head-tail junction, resulting in changes in sedimentation coefficient, ATPase activity, and orientation of heads. *J. Biol. Chem.* **260**, 4810-4817.
13. Elliott, A. & Offer, G. (1978). Shape and flexibility of the myosin molecule. *J. Mol. Biol.* **123**, 505-519.
14. Offer, G. (1990). Skip residues correlate with bends in the myosin tail. *J. Mol. Biol.* **216**, 213-218.

15. Liu, J., Wendt, T., Taylor, D. & Taylor, K. (2003). Refined model of the 10 S conformation of smooth muscle myosin by cryo-electron microscopy 3D image reconstruction. *J. Mol. Biol.* **329**, 963-972.
16. Wendt, T., Taylor, D., Messier, T., Trybus, K. M. & Taylor, K. A. (1999). Visualization of head-head interactions in the inhibited state of smooth muscle myosin. *J. Cell Biol.* **147**, 1385-1389.
17. Wendt, T., Taylor, D., Trybus, K. M. & Taylor, K. (2001). Three-dimensional image reconstruction of dephosphorylated smooth muscle heavy meromyosin reveals asymmetry in the interaction between myosin heads and placement of subfragment 2. *Proc. Natl. Acad. Sci. USA* **98**, 4361-4366.
18. Woodhead, J. L., Zhao, F. Q., Craig, R., Egelman, E. H., Alamo, L. & Padrón, R. (2005). Atomic model of a myosin filament in the relaxed state. *Nature* **436**, 1195-1199.
19. Tama, F., Feig, M., Liu, J., Brooks, C. L. & Taylor, K. A. (2005). The requirement for mechanical coupling between head and S2 domains in smooth muscle myosin ATPase regulation and its implications for dimeric motor function. *J. Mol. Biol.* **345**, 837-854.
20. Sheng, S. T., Gao, Y., Khromov, A. S., Somlyo, A. V., Somlyo, A. P. & Shao, Z. F. (2003). Cryo-atomic force microscopy of unphosphorylated and thiophosphorylated single smooth muscle myosin molecules. *J. Biol. Chem.* **278**, 39892-39896.
21. Burgess, S. A., Walker, M. L., Thirumurugan, K., Trinick, J. & Knight, P. J. (2004). Use of negative stain and single-particle image processing to explore dynamic properties of flexible macromolecules. *J. Struct. Biol.* **147**, 247-258.
22. Thirumurugan, K., Sakamoto, T., Hammer, J. A., Sellers, J. R. & Knight, P. J. (2006). The cargo-binding domain regulates structure and activity of myosin 5. *Nature* **442**, 212-215.
23. Burgess, S. A., Walker, M. L., White, H. D. & Trinick, J. (1997). Flexibility within myosin heads revealed by negative stain and single-particle analysis. *J. Cell Biol.* **139**, 675-681.
24. Burgess, S., Walker, M., Wang, F., Seller, J. R., White, H. D., Knight, P. J. & Trinick, J. (2002). The prepower stroke conformation of myosin V. *J. Cell Biol.* **159**, 983-991.
25. Offer, G. & Knight, P. (1996). The structure of the head-tail junction of the myosin molecule. *J. Mol. Biol.* **256**, 407-416.
26. Onishi, H., Wakabayashi, T., Kamata, T. & Watanabe, S. (1983). Electron-microscopic studies of myosin molecules from chicken gizzard muscle. 2. The effect of thiophosphorylation of the 20k-Dalton light chain on the ATP-induced change in the conformation of myosin monomers. *J. Biochem. (Tokyo)* **94**, 1147-1154.
27. Dominguez, R., Freyzon, Y., Trybus, K. M. & Cohen, C. (1998). Crystal structure of a vertebrate smooth muscle myosin motor domain and its complex with the essential light chain: Visualization of the pre-power stroke state. *Cell* **94**, 559-571.
28. Houdusse, A., Szent-Györgyi, A. G. & Cohen, C. (2000). Three conformational states of scallop myosin S1. *Proc. Natl. Acad. Sci. USA* **97**, 11238-11243.

29. Gourinath, S., Himmel, D. M., Brown, J. H., Reshetnikova, L., Szent-Gyorgyi, A. G. & Cohen, C. (2003). Crystal structure of scallop myosin S1 in the pre-power stroke state to 2.6 Å resolution: Flexibility and function in the head. *Structure* **11**, 1621-1627.
30. Ikebe, M., Ikebe, R., Kamisoyama, H., Reardon, S., Schwonek, J. P., Sanders, C. R. & Matsuura, M. (1994). Function of the NH₂-terminal domain of the regulatory light-chain on the regulation of smooth-muscle myosin. *J. Biol. Chem.* **269**, 28173-28180.
31. Wu, X. D., Clack, B. A., Zhi, G., Stull, J. T. & Cremo, C. R. (1999). Phosphorylation-dependent structural changes in the regulatory light chain domain of smooth muscle heavy meromyosin. *J. Biol. Chem.* **274**, 20328-20335.
32. Cremo, C. R., Wang, F., Facemyer, K. & Sellers, J. R. (2001). Phosphorylation-dependent regulation is absent in a nonmuscle heavy meromyosin construct with one complete head and one head lacking the motor domain. *J. Biol. Chem.* **276**, 41465-41472.
33. Stafford, W. F., Jacobsen, M. P., Woodhead, J., Craig, R., O'Neill-Hennessey, E. & Szent-Györgyi, A. G. (2001). Calcium-dependent structural changes in scallop heavy meromyosin. *J. Mol. Biol.* **307**, 137-147.
34. Olney, J. J., Sellers, J. R. & Cremo, C. R. (1996). Structure and function of the 10S conformation of smooth muscle myosin. *J. Biol. Chem.* **271**, 20375-20384.
35. Trybus, K. M., Freyzon, Y., Faust, L. Z. & Sweeney, H. L. (1997). Spare the rod, spoil the regulation: Necessity for a myosin rod. *Proc. Natl. Acad. Sci. USA* **94**, 48-52.
36. Rimm, D. L., Sinard, J. H. & Pollard, T. D. (1989). Location of the head tail junction of myosin. *J. Cell Biol.* **108**, 1783-1789.
37. Salzameda, B., Facemyer, K. C., Beck, B. W. & Cremo, C. R. (2006). The N-terminal lobes of both regulatory light chains interact with the tail domain in the 10S inhibited conformation of smooth muscle myosin. *J. Biol. Chem.* **281**, 38801-38811.
38. Quinlan, R. A. & Stewart, M. (1987). Crystalline tubes of myosin subfragment-2 showing the coiled-coil and molecular interaction geometry. *J. Cell Biol.* **105**, 403-415.
39. Hvidt, S., Nestler, F. H. M., Greaser, M. L. & Ferry, J. D. (1982). Flexibility of myosin rod determined from dilute-solution viscoelastic measurements. *Biochemistry* **21**, 4064-4073.
40. Tonino, P., Simon, M. & Craig, R. (2002). Mass determination of native smooth muscle myosin filaments by scanning transmission electron microscopy. *J. Mol. Biol.* **318**, 999-1007.
41. Knight, P. J. (1996). Dynamic behaviour of the head-tail junction of myosin. *J. Mol. Biol.* **255**, 269-274.
42. Lauzon, A. M., Fagnant, P. M., Warshaw, D. M. & Trybus, K. M. (2001). Coiled-coil unwinding at the smooth muscle myosin head-rod junction is required for optimal mechanical performance. *Biophys. J.* **80**, 1900-1904.
43. Trybus, K. M. (1994). Regulation of expressed truncated smooth-muscle myosins - role of the essential light-chain and tail length. *J. Biol. Chem.* **269**, 20819-20822.

44. Mazhari, S. M., Selser, C. T. & Cremona, C. R. (2004). Novel sensors of the regulatory switch on the regulatory light chain of smooth muscle myosin. *J. Biol. Chem.* **279**, 39905-39914.
45. Persechini, A. & Hartshorne, D. J. (1983). Ordered phosphorylation of the 20000 molecular-weight light-chains of smooth-muscle myosin. *Biochemistry* **22**, 470-476.
46. Sobieszek, A. & Bremel, R. D. (1975). Preparation and properties of vertebrate smooth-muscle myofibrils and actomyosin. *Eur. J. Biochem.* **55**, 49-60.
47. Frederiksen, D. W. & Rees, D. D. (1982). Preparation of smooth-muscle myosin. *Methods Enzymol.* **85**, 292-298.
48. Sellers, J. R., Eisenberg, E. & Adelstein, R. S. (1982). The binding of smooth-muscle heavy-meromyosin to actin in the presence of ATP - effect of phosphorylation. *J. Biol. Chem.* **257**, 13880-13883.
49. Knight, P. & Trinick, J. (1984). Structure of the myosin projections on native thick filaments from vertebrate skeletal-muscle. *J. Mol. Biol.* **177**, 461-482.
50. Elliott, A., Offer, G. & Burridge, K. (1976). Electron-microscopy of myosin molecules from muscle and non-muscle sources. *Proc. R. Soc. Lond. B Biol. Sci.* **193**, 45-53.
51. Penczek, P., Radermacher, M. & Frank, J. (1992). 3-Dimensional reconstruction of single particles embedded in ice. *Ultramicroscopy* **40**, 33-53.
52. Frank, J. (1996). *Three-Dimensional Electron Microscopy of Macromolecular Assemblies*, Academic Press, San Diego.
53. Fraser, R. D. B. & MacRae, T. P. (1973). *Conformation in Fibrous Proteins and Related Synthetic Polypeptides*, Academic Press, New York.
54. Yanagisawa, M., Hamada, Y., Katsuragawa, Y., Imamura, M., Mikawa, T. & Masaki, T. (1987). Complete primary structure of vertebrate smooth-muscle myosin heavy-chain deduced from its complementary-DNA sequence - implications on topography and function of myosin. *J. Mol. Biol.* **198**, 143-157.
55. Offer, G., Hicks, M. R. & Woolfson, D. N. (2002). Generalized Crick equations for modeling noncanonical coiled coils. *J. Struct. Biol.* **137**, 41-53.

FIGURE LEGENDS

Fig. 1. Smooth muscle myosin.

(A) Structural organization of full length smooth muscle myosin heavy chain (from chicken gizzard) and HMM fragment used in this study. The IQ domains (blue and yellow), that bind the ELC and RLC respectively, lie between the motor domain (grey, residues 1-791) and the coiled-coil domain (red). Positions and residue numbers of the nominal skip residues in the coiled-coil are indicated. (B) Space-filling model of HMM from 2-D crystals on lipid monolayers. Heavy chain motor and lever domains: grey, coiled coil: red, ELCs: blue, RLCs: yellow. Converter subdomain: orange (visible only in blocked head in this view). Blocked head is shown in darker colours. Model derived from PDB file 1I84¹⁷ with complete chicken skeletal muscle RLCs (coordinates kindly supplied by I. Rayment) added by superposition in Swiss PDB Viewer, which also completed partial side chains. The RLCs were then replaced by a homology model of the chicken gizzard smooth muscle RLC created using SwissModel. Image prepared using PyMOL (DeLano Scientific).

Fig. 2. Smooth muscle myosin and HMM molecules in negative stain.

(A) a field of whole myosin; (B) a gallery of whole myosin showing: (upper row) separate heads on a compactly folded tail and (upper left panel) a completely unfolded molecule for comparison; (middle row) side views of compactly folded molecules; (lower row) more common face views of compactly folded molecules; (C) a field of HMM; (D) a gallery of (upper two rows) open and (lower row) compact HMM molecules. Scale bar in (C) 100 nm; (D) 50 nm.

Fig. 3. Head region of compact HMM images.

(A-C) Examples of averaged images from classes showing compact structure. (D-F) Examples showing less regular compact structure. The free-head motor domain (arrows in D, E) often appears different from that in the compact form but occasionally so does the blocked head motor domain, producing a less asymmetric structure (F). Numbers at lower right of each panel are the number of images assigned to each class. Panels are 41 nm wide.

Fig. 4. Analysis of non-compact HMM images.

(A) Scatter plot of angles between the tail and left and right heads. HMM images in which the tail was visible in raw micrographs and showing the two heads separated ($n=411$), were selected, aligned manually (see Methods) and angles measured as shown in the cartoon. (B) Averages of the images contained in the corresponding 25° bins near the origin of the scatter plot (boxed areas in A). The panel nearest the origin is an average of compact molecules from single-particle processing, as there are few molecules in this region of the scatter plot. The number of images in each average is shown. Panels are 51 nm wide.

Fig. 5. Head region of whole myosin molecules.

(A-C) Examples of classes showing compact molecules. (D) Side view of compact molecules. (E-F) Less compact molecules. In (B), arrow points to the coalesced segments of tail, and arrowhead indicates the prominent spot beside the blocked head lever domain. In (E), the white arrow points to the free head motor domain. The number of images in each average is shown. Panels are 41 nm wide

Fig. 6. Path of the tail in the compact myosin head.

Left panel is the average of 138 myosin molecules, the central panel the average of 226 HMM molecules. The right panel shows a subtraction image between myosin and HMM. Arrowhead and arrow indicate the position of the prominent spot beside the blocked head lever domain and the coalesced tail respectively. Panels are 41 nm wide.

Fig. 7. Characteristics of the tail.

Representative class averages showing flexibility of the tail of (A) HMM and (C) myosin molecules, after alignment of the heads (myosin and HMM co-aligned). The middle panel in each row shows the mean position of the tail. Numbers in lower right indicate the chord angle of the tail at a position 25.7 nm (50 pixels) along the tail from its emergence point from the head (i.e. the fulcrum). The angle is defined in relation to the path of the tail between the head-tail junction and the fulcrum, see cartoon at right). (B)

and (D): Histograms of tail angles for HMM and myosin, respectively. (E) Examples showing the range of structures of myosin tails after alignment of the whole molecule (i.e. including the tail). Arrowhead and arrow indicate the first bend and tip of tail respectively; asterisk marks a class with the three tail segments coalesced throughout their length; numbers are class size. Panels are 41 nm wide.

Fig. 8. Path of the tail and lengths of tail segments.

(A) Diagram showing the path of the tail superposed on the model of the heads used in Fig. 1B. The black arrowhead indicates the second bend, and the black arrow the coalesced tail region, as in Figs 5 & 6. RLC Cys108 used in crosslinking experiments is coloured red and emphasized by the bent red arrow and X. The path of the third tail segment has been displaced to the left locally in order to expose it. The three segments of the folded tail are numbered, and the calculated residue numbers of the two bends in the heavy chain sequence are shown. (B) Lengths of segments of the myosin tail compared with lengths expected if bends were at skip residues. Lengths were obtained from 10 image averages that included 467 molecules. Five measured lengths of the part of segment 3 that extends beyond the other segments clustered around 6.6 nm, whereas the rest appeared up to a few nm shorter, probably due to flexibility and weaker delineation of this feature. Therefore segment 3 length and overall tail length derive from these five classes. Expected lengths are calculated for a coiled coil which starts at Pro848 and ends at Pro1939, assuming 0.1485 nm per residue⁵³, and bends at skip residues assigned as Gln1198 and Gln1591⁵⁴. Bending near skip residue Lys1816 was not detected. The shift in the hydrophobic seam produced by a skip residue occurs by two hendecad ‘stutters’ that in principle can be several heptads apart⁵⁵. Inspection of the sequence indicates that in each case the stutters are consecutive and very close to the nominal skip sites.

Figure 1

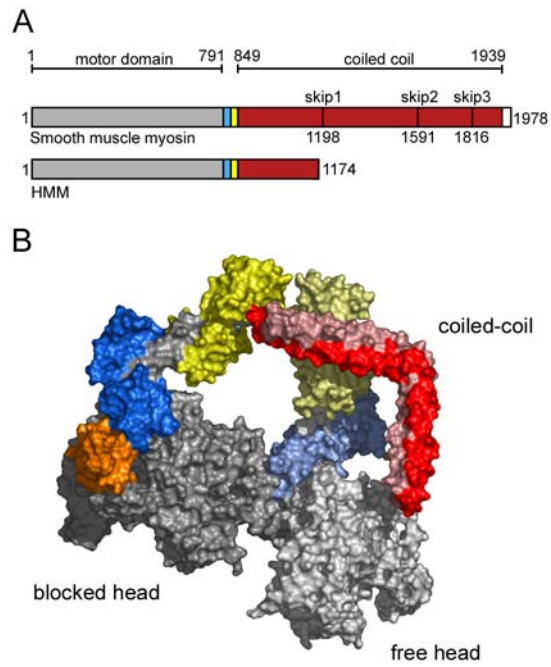


Figure 2

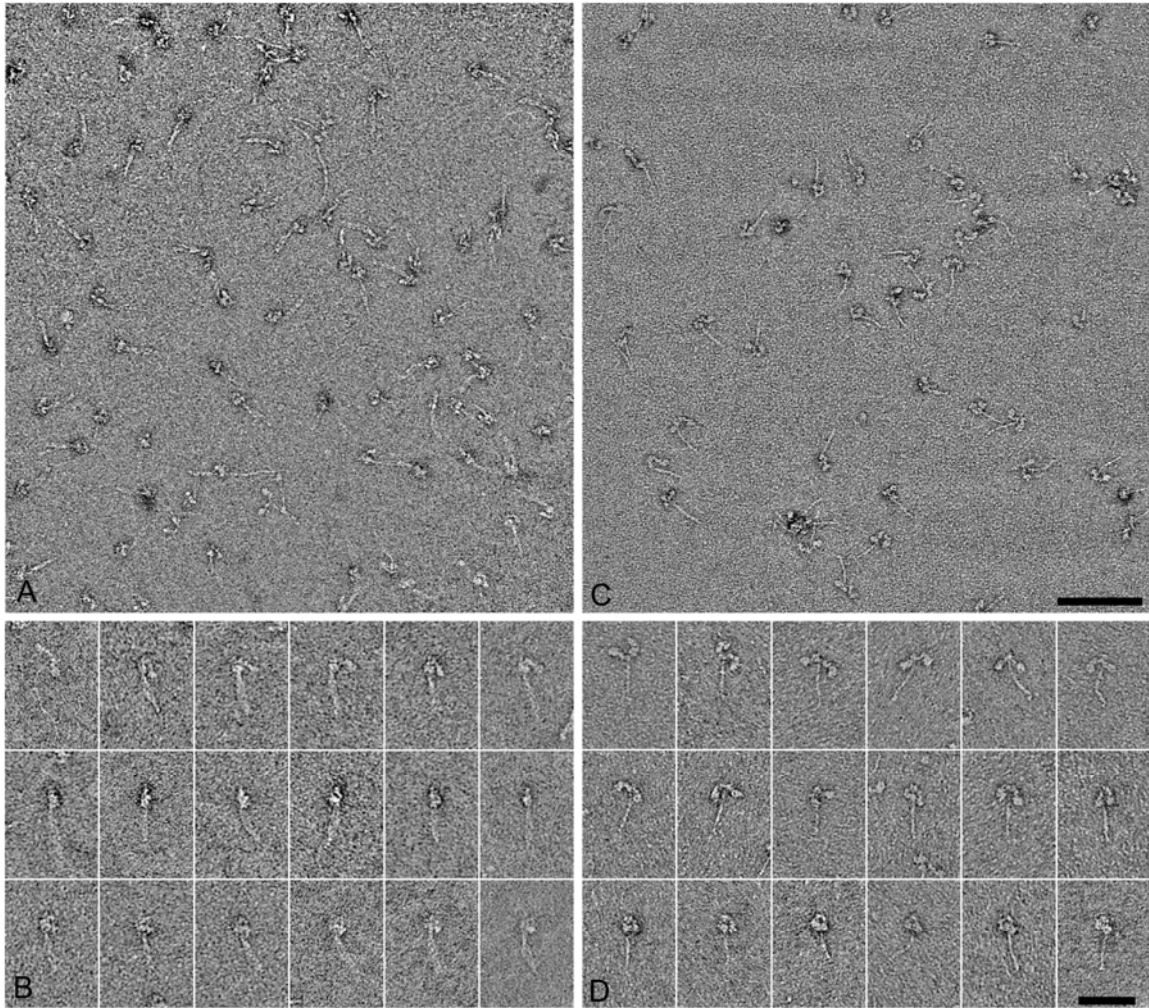


Figure 3

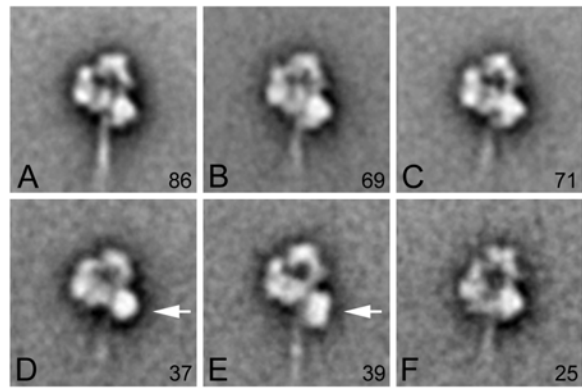


Figure 4

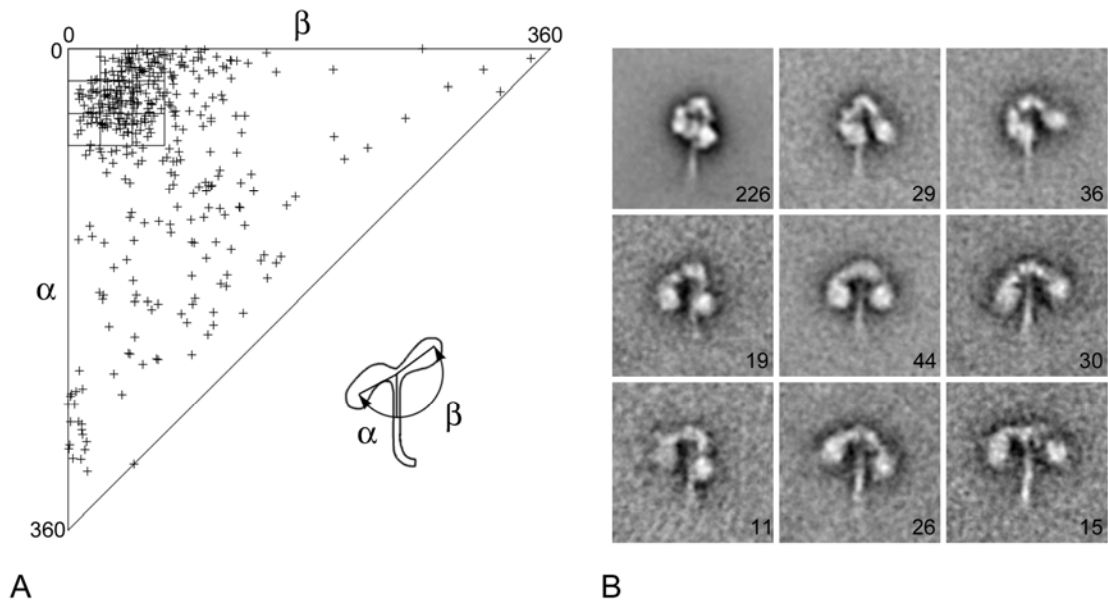


Figure 5

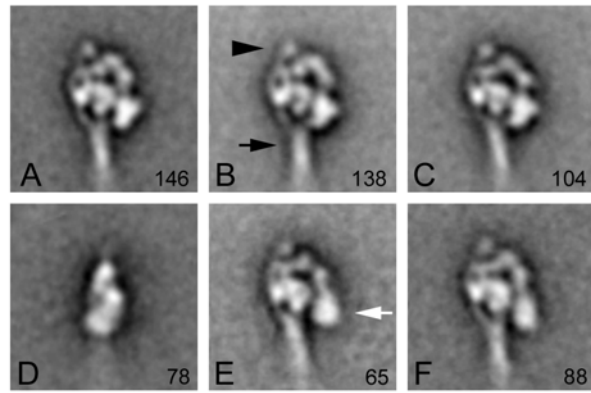


Figure 6

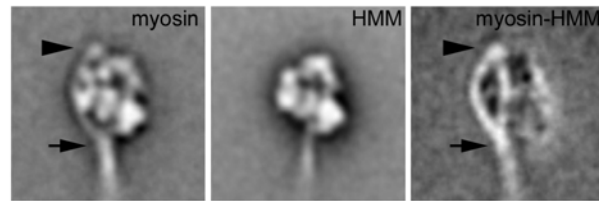


Figure 7

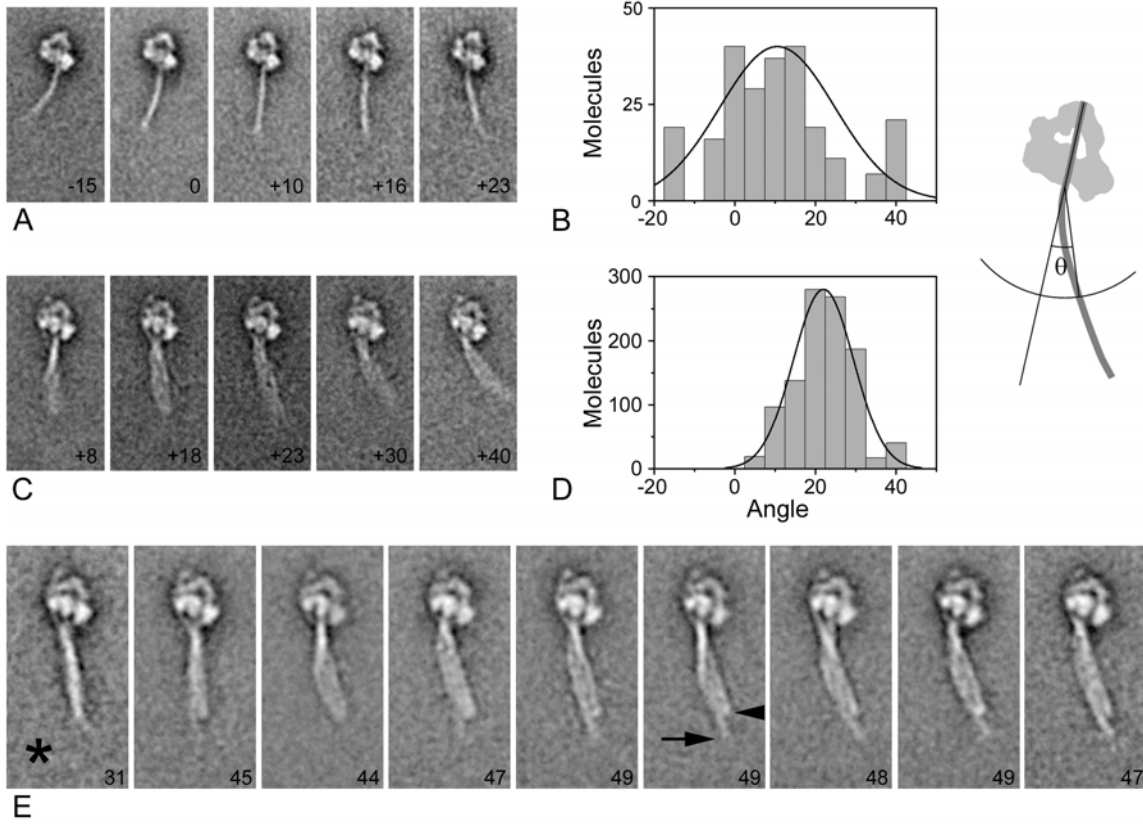
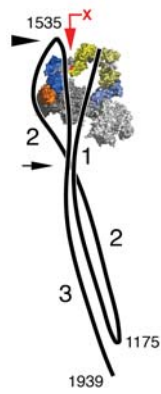


Figure 8



Segment	Expected length (nm)	Measured length (nm \pm SEM)	Inferred number of residues	Inferred sequence limits of segment
First	52.0	48.5 \pm 0.3	326	848-1175
Second	58.4	53.6 \pm 0.3	361	1175-1535
Third	51.7	58.7 \pm 0.5	395	1535-1939
Overall	162.0	160.5 \pm 1.1	1082	848-1939

SUPPLEMENTARY MATERIALS

The following movies are compiled to display the diversity of structures present in the micrographs. The frames are arranged in an ascending and descending angular sequence rather than in random order to make each movie easier to follow, but this should not be taken to suggest that individual molecules execute pendulum-like movements in solution.

Movie 1: *Conformations of the free head of whole, folded smooth muscle myosin.*

Images were aligned and classified using features only in the head region, so the flexible tail is smeared out. To create the movie, class averages were arranged in order of the x-axis position of the free head motor domain, and repeated in reverse order to complete the movie.

Movie 2: *Flexibility of the tail of smooth muscle HMM.*

Images of compact molecules were co-aligned with those of whole myosin (see Movie 3) using features only of the head region, and then classified using a wedge-shaped mask centred on the point of emergence of the tail from the heads and extending almost to the tip of the tail. To make the movie, the image averages were arranged in order of tail angle, measured as shown in Fig. 7, and repeated in reverse order to complete the movie.

Movie 3: *Flexibility of the tail of whole, folded smooth muscle myosin.*

Images of compact molecules were co-aligned with those of HMM (see Movie 2) using features only of the head region, and classified using the same wedge-shaped mask used for HMM. To make the movie, the image averages were arranged in order of tail angle, measured as shown in Fig. 7, and repeated in reverse order to complete the movie.

Movie 4: *Structure of the folded tail of whole, smooth muscle myosin.*

Smooth muscle myosin images were aligned using features only from the head region and classified with a longer wedge mask than in Movie 3, and thus better show the structure of the distal part of the tail. To make the movie, the image averages were arranged in order of tail angle, measured as shown in Fig. 7, and repeated in reverse order to complete the movie.